

A comparative study on radiation reliability of composite channel InP high electron mobility transistors

Jia-Jia Zhang(张佳佳), Peng Ding(丁芃), Ya-Nan Jin(靳雅楠), Sheng-Hao Meng(孟圣皓), Xiang-Qian Zhao(赵向前), Yan-Fei Hu(胡彦飞), Ying-Hui Zhong(钟英辉), and Zhi Jin(金智)

Citation: Chin. Phys. B, 2021, 30 (**7**): 070702. DOI: 10.1088/1674-1056/abe2fd
Journal homepage: http://cpb.iphy.ac.cn; http://iopscience.iop.org/cpb

What follows is a list of articles you may be interested in

Magnetic shielding property for cylinder with circular, square, and equilateral triangle holes

Si-Yuan Hao(郝思源), Xiao-Ping Lou(娄小平), Jing Zhu(祝静), Guang-Wei Chen(陈广伟), and Hui-Yu Li(李慧宇)
Chin. Phys. B, 2021, 30 (**6**): 060702. DOI: 10.1088/1674-1056/abeeee

Efficient sampling for decision making in materials discovery

Yuan Tian(田原), Turab Lookman, and Dezhen Xue(薛德祯)
Chin. Phys. B, 2021, 30 (**5**): 050705. DOI: 10.1088/1674-1056/abf12d

Theoretical analysis and experimental validation of radial cascaded composite ultrasonic transducer

Xiao-Yu Wang(王晓宇), Zhi-Xin Yu(余芷欣), Jing Hu(胡静), and Shu-Yu Lin(林书玉)
Chin. Phys. B, 2021, 30 (**4**): 040701. DOI: 10.1088/1674-1056/abd399

Coupling analysis of transmission lines excited by space electromagnetic fields based on time domain hybrid method using parallel technique

Zhi-Hong Ye(叶志红), Xiao-Lin Wu(吴小林), Yao-Yao Li(李尧尧)
Chin. Phys. B, 2020, 29 (**9**): 090701. DOI: 10.1088/1674-1056/ab96a6

Simulation study of high voltage GaN MISFETs with embedded PN junction

Xin-Xing Fei(费新星), Ying Wang(王颖), Xin Luo(罗昕), Cheng-Hao Yu(于成浩)
Chin. Phys. B, 2020, 29 (**8**): 080701. DOI: 10.1088/1674-1056/ab90f7

A comparative study on radiation reliability of composite channel InP high electron mobility transistors*

Jia-Jia Zhang(张佳佳)[1], Peng Ding(丁芃)[2], Ya-Nan Jin(靳雅楠)[1], Sheng-Hao Meng(孟圣皓)[1], Xiang-Qian Zhao(赵向前)[1], Yan-Fei Hu(胡彦飞)[3], Ying-Hui Zhong(钟英辉)[1,†], and Zhi Jin(金智)[2]

[1] *School of Physics and Microelectronics, Zhengzhou University, Zhengzhou* 450001, *China*
[2] *Institute of Microelectronics, Chinese Academy of Sciences, Beijing* 100029, *China*
[3] *Microelectronics Institute, Xidian University, Xi'an* 710071, *China*

(Received 3 November 2020; revised manuscript received 7 January 2021; accepted manuscript online 4 February 2021)

This paper proposes a reasonable radiation-resistant composite channel structure for InP HEMTs. The simulation results show that the composite channel structure has excellent electrical properties due to increased modulation doping efficiency and carrier confinement. Moreover, the direct current (DC) and radio frequency (RF) characteristics and their reliability between the single channel structure and the composite channel structure after 75-keV proton irradiation are compared in detail. The results show that the composite channel structure has excellent radiation tolerance. Mechanism analysis demonstrates that the composite channel structure weakens the carrier removal effect. This phenomenon can account for the increase of native carrier and the decrease of defect capture rate.

Keywords: proton irradiation, composite channel, InP HEMTs, TCAD modeling

PACS: 07.05.Tp, 72.80.Ey, 72.20.Jv, 95.30.Gv **DOI:** 10.1088/1674-1056/abe2fd

1. Introduction

In recent years, high-precision sensing and high-quality communication have imposed huge requirements on the operating frequency of integrated circuits, which has increased from W-band to G-band or even terahertz.[1,2] A variety of techniques are adopted to extend the Moore' law and improve the devices' frequency characteristics, such as novel structures[3,4] and fabrication technology.[5] The InP-based high electron mobility transistors (HEMTs) have demonstrated high carrier sheet density, peak drift velocity, and low-field mobility, and the recorded frequency characteristics have exceeded 1 THz.[6] Therefore, they are recognized as a promising candidate for power amplifiers (PAs) and low noise amplifiers (LNAs) of upcoming THz satellite communication and deep space detection systems.[7–10]

When electronic equipment operates in harsh space environment, its performance deterioration and even abnormality result from various high energetic particles and cosmic rays. Therefore, it is essential to understand the radiation reliability of these devices. Since III–V HEMTs are not sensitive to ionization effects, researchers primarily focus on the displacement effects caused by irradiation. So far, the displacement effects of GaN and GaAs HEMTs have been extensively studied. Typical features are the positive shift of threshold voltage, degradation of transconductance, current, operating frequency, and gain.[11–18] Besides, the related literature demonstrates that a large value of conduction band offset correlates with greater tolerance of radiation damage.[19,20]

However, there are few studies on the proton irradiation of InP HEMTs.[21,22] The present work presents a reasonable radiation-resistant composite channel structure for InP HEMTs. A combination of SRIM and ISE-TCAD is used to simulate the radiation reliability of the composite channel structure InP HEMTs. The trap model and the ionized impurity scattering model account for the carrier removal and mobility degradation caused by irradiation. And finally, an understandable explanation for the better radiation reliability of the composite channel is presented.

2. Modeling

2.1. Device structure

Figures 1(a) and 1(b) show the schematic cross-sections of the traditional single channel structure and the composite channel structure InP HEMTs, respectively. These two device structures possess almost the same epitaxial layers apart from the channel layer. The entire epilayers of single channel structure from bottom to top consist of an InP semi-insulating substrate, a 500-nm-thick $In_{0.52}Al_{0.48}As$ (InAlAs) buffer layer,

*Project supported by the National Natural Science Foundation of China (Grant No. 11775191), the Natural Science Foundation of Henan Province, China (Grant No. 202300410379), the Promotion Funding for Excellent Young Backbone Teacher of Henan Province, China (Grant No. 2019GGJS017), Key Technologies Research and Development Program of Henan Province, China (Grant No.202102210321), and the Promotion Project for Physics Discipline in Zhengzhou University, China (Grant No. 2018WLTJ01).

†Corresponding author. E-mail: zhongyinghui@zzu.edu.cn

© 2021 Chinese Physical Society and IOP Publishing Ltd

15-nm-thick $In_{0.52}Al_{0.48}As$ (InGaAs) channel layer, 5-nm-thick InAlAs spacer layer, a δ-doping plane with a concentration of 5×10^{12} cm^{-2}, 10-nm-thick InAlAs barrier layer, uppermost 30-nm-thick heavily-doped InGaAs cap layer with a doping concentration of 3×10^{19} cm^{-3}. The composite channel contains 3-nm-thick InGaAs layer, 2-nm-thick InAs layer, and 10-nm-thick $In_{0.53}(Al_{0.3}Ga_{0.7})_{0.47}As$ (InAlGaAs) layer. All InAlAs and InGaAs layers are lattice matched with InP substrate as well as InAlGaAs. The gate length is set to be 100 nm, and both gate–source distance and gate–drain distance are 1.0 μm.

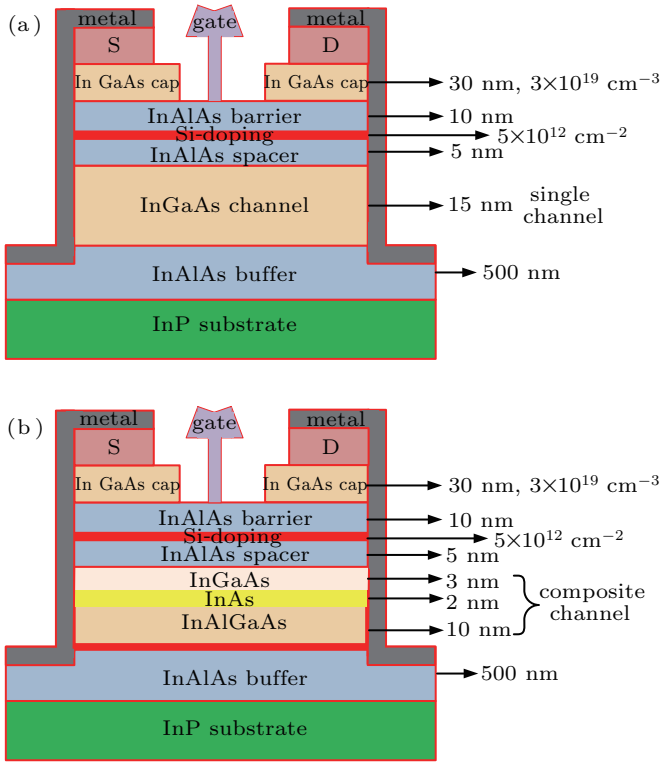


Fig. 1. Schematic cross-sections of InP HEMTs: (a) single channel structure and (b) composite channel structure.

2.2. Physical model

The accurate physical models are used to simulate the device characteristics, including hydrodynamic transport model, Shockley–Read–Hall recombination, Auger recombination, radiative recombination, density gradient model, and mobility high-field saturation model. Detailed model and calibration refer to the counterparts previous work.[23,24] Moreover, the trap model is employed to introduce the radiation damage into device simulation. And the self-consistent coupling of Poisson equation, current continuity equations, current density equations are given as follows:[25]

$$\nabla^2\varphi = -\frac{q}{\varepsilon}\left[p - n + N_{\rm D}^{+} - N_{\rm A}^{-} - \rho_{\rm trap}\right], \tag{1}$$

$$\frac{\partial n}{\partial t} = \frac{1}{q}\nabla\cdot J_n, \quad \frac{\partial p}{\partial t} = \frac{1}{q}\nabla\cdot J_p, \tag{2}$$

$$J_n = -q\mu_n n\nabla\Phi_n, \quad J_p = -q\mu_p p\nabla\Phi_p, \tag{3}$$

where φ is the electrostatic potential, q is the elementary charge, ε is the material permittivity, n is the electron density, p is the hole density, $N_{\rm D}^{+}$, $N_{\rm A}^{-}$, and $\rho_{\rm trap}$ are the ionized donor, acceptor density, and trap density, J_n and J_p are the current densities, μ_n and μ_p are the carrier mobilities, respectively, Φ_n and Φ_p are the quasi-Fermi levels.

2.3. Vacancy profile

Displacement-related point defects are considered the primary damage mechanism that influences device performance in proton-irradiated InP HEMTs.[12,13,20] Energetic protons transfer part of their kinetic energy to the lattice atoms through non-ionizing energy loss (NIEL). This energy displaces atoms from their lattice sites and creates charged defect centers. According to the number of vacancies created in the given depth after energetic proton incidence, we can calculate the densities of vacancy at different proton fluences. Here we consider only the influence of As vacancies on InP HEMT, because As vacancies act as acceptor defects and the influence of donor defects on the device can be ignored.[26,27] Figure 2 shows the As vacancy densities created near the heterojunction versus 75-keV proton fluence, calculated by SRIM. Under the same fluence, there is no significant difference between the vacancy density of the barrier layer and the channel layer. In addition, the 75-keV proton NIEL is about 2.3 MeV·cm^2/g in both of InP HEMT structures.

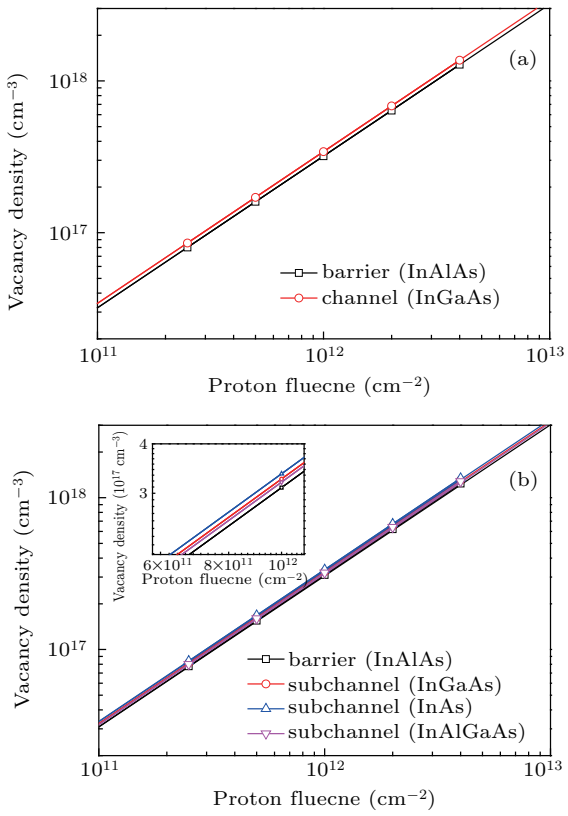


Fig. 2. Vacancy density near heterojunction *versus* proton fluence of (a) single channel structure and (b) composite channel structure.

2.4. Results and discussion

DC transfer characteristics of both HEMTs at a drain voltage (V_{DS}) of 1.5 V are shown in Fig. 3(a). The composite channel structure exhibits over 1200 mS/mm of peak transconductance ($g_{m,max}$) and 873 mA/mm of saturation current ($I_{DS,sat}$). Compared with single channel structure, composite channel structure significantly increases peak transconductance and saturation current. Besides, under the same Schottky barrier, the composite channel structure's threshold voltage (V_{th}) is more negative. The reason will be explained in detail below. Figures 3(b) and 3(c) show the small-signal RF characteristic of both HEMTs at $V_{DS} = 1.5$ V and gate–source voltage (V_{GS}) biases around the points with peak transconductance. In a low-frequency band, the current gain (H_{21}) and the maximum available/stable power gain (MAG/MSG) curves are flat. With the increase of frequency, the current gain decreases by −20 dB /decade, while the power gain decreases by two slopes, the stability factor $K = 1$ where the slope changes from −10 dB/decade (MSG) to −20 dB/decade (MAG). Note that the current gain cutoff frequency (f_T) and maximum oscillation frequency (f_{max}) of the composite channel structure reach 440 GHz and 930 GHz, respectively. The detailed device characteristics are summarized in Table 1.

The improved characteristics of the composite channel structure can be explained by simulating the conduction band and the two-dimensional electron gas density of the heterojunction, and the results are shown in Fig. 4. It can be intuitively seen that the single channel structure forms a triangular-like potential well near the heterojunction, and the electrons are confined mainly in this potential well while the composite channel structure electrons are confined primarily in the InAs subchannel with higher mobility. Besides, the composite channel structure results in an apparent increase in modulation efficiency expressed by higher sheet density of two-dimensional electron gas density because of the insertion of InAs. This directly leads the threshold voltage to shift negatively.[28] In other words, the higher carrier density and mobility of the composite channel structure result in excellent DC and RF characteristics.

Table 1. Electrical characteristics of both HEMTs.

	V_{th} (V)	$I_{DS,sat}$ (mA/mm)	$g_{m,max}$ (mS/mm)	f_T (GHz)	f_{max} (GHz)
Single channel	–0.36	527	744	240	570
Composite channel	–0.68	873	1204	440	930

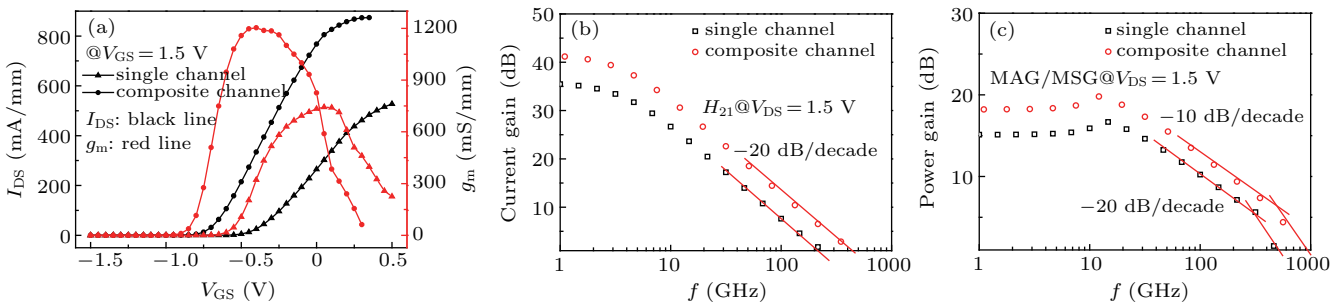


Fig. 3. Electrical characteristics of both HEMTs: (a) transfer characteristics, (b) current gain, and (c) power gain.

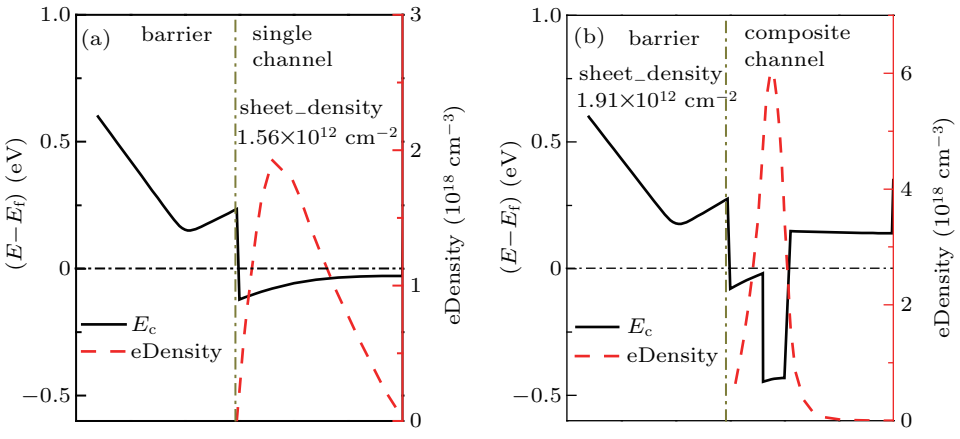


Fig. 4. Conduction band diagrams and electron density profiles of both HEMTs: (a) single channel structure, (b) composite channel structure.

The transfer characteristics of both HEMTs without and with the irradiation of protons are investigated. However, figure 5 shows the case of only non-irradiation, proton fluence of 5.0×10^{11} cm^{-2} and 2.0×10^{12} cm^{-2} for clarity. With the increase of the proton fluence, both structures exhibit different degrees of degradation, mainly in reducing transconductance and current, the threshold voltage shifts toward more positive value. This is consistent with the explanation that the radiation yields the acceptor defects near the heterojunction.[18]

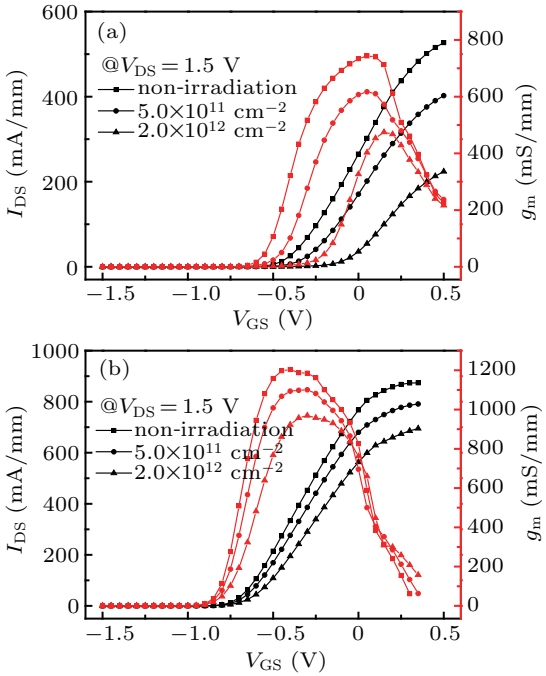


Fig. 5. Transfer characteristics of both HEMTs: (a) single channel structure and (b) composite channel structure at different proton fluences.

The relationships between the normalized critical parameters and different proton fluences are shown in Fig. 6. The normalized value is adopted here for comparison, in order to eliminate the difference between the characteristics of both structures and more intuitively reflect the degradation degree of critical parameters by the irradiation fluence. The normalized DC parameters, such as threshold voltage, peak transconductance, and saturation current show that the composite channel structure leads to better radiation reliability. The reason will be explained below in terms of the degradation of carrier density and mobility. Within the simulated proton fluence, the higher the fluence, the more pronounced the advantage of the composite channel structure is. To make the simulation results more convincing, we compare the single channel structure's current degradation rate with those of other III–V HEMT irradiation experiments where the methods in the literature are adopted,[19] and the results are shown in Fig. 6(d). The current degradation rate obtained by simulation is of the same order of magnitude as the experimental value, and there is no significant difference.

Figures 6(e) and 6(f) show the radiation fluence dependence of the cut-off frequency and the maximum oscillation frequency. Note that the RF parameters do not change significantly like the DC parameters in the simulated fluence range, especially the maximum oscillation frequency. In fact, the frequency parameters are inversely proportional to the carrier transport time in the channel, which are expressed as[29]

$$f_{\mathrm{T}} = \frac{1}{2\pi(\tau_{\mathrm{ex}} + L_{\mathrm{g}}/v_{\mathrm{d}})}, \tag{4}$$

$$f_{\max} = \frac{f_{\mathrm{T}}}{2}\sqrt{\frac{R_{\mathrm{ds}}}{R_{\mathrm{g}} + R_{\mathrm{i}}}}, \tag{5}$$

where L_{g} is the gate length, v_{d} is the electron drift velocity, τ_{ex} is the extrinsic delay time, R_{ds} is the channel resistance, R_{g} is the gate contact resistance, and R_{i} is the Schottky junction resistance. Regardless of parasitic effects, the frequency parameters should be closely related to the drift velocity under a certain gate length. When the drift velocity reaches a saturation value, the Coulomb scattering of the defects introduced by the irradiation no longer dominates unless radiation fluence is very high. The Coulomb scattering caused by charged defects is an important cause of DC degradation. In other words, the effect of radiation on RF parameters lags DC parameters. Related studies show that the degradation of RF response is due to impedance mismatches caused by changes in resistance and capacitance.[18]

Carrier removal and mobility reduction are regarded as the causes of DC degradation of irradiated HEMTs.[30] To illustrate the higher reliability of the composite channel structure in terms of DC parameters, we extract the two-dimensional electron gas sheet density (n_{s}) and mobility (μ) of the two structures under different irradiation fluences, and the results are shown in Fig. 7. The normalized form is still used here for the convenience of comparison. The two-dimensional electron gas density has a linear relationship with the radiation fluence. According to the Coulomb scattering model of charged defects, the mobility is more sensitive to radiation. Mobility degrades rapidly at low fluence, but at high fluence the degradation value tends to be saturated. It is consistent with the irradiation experiment of the GaN-based two-dimensional electron gas system.[31] Although the mobility degradations of the two structures are almost the same due to a similar defect density (Fig. 2), the carrier removal rate of the composite channel structure is significantly lower than that of the single channel structure. This indicates that comparing with the single channel structure, the improvement of the radiation reliability of the composite channel is reflected mainly in the weakening of the carrier removal effect.

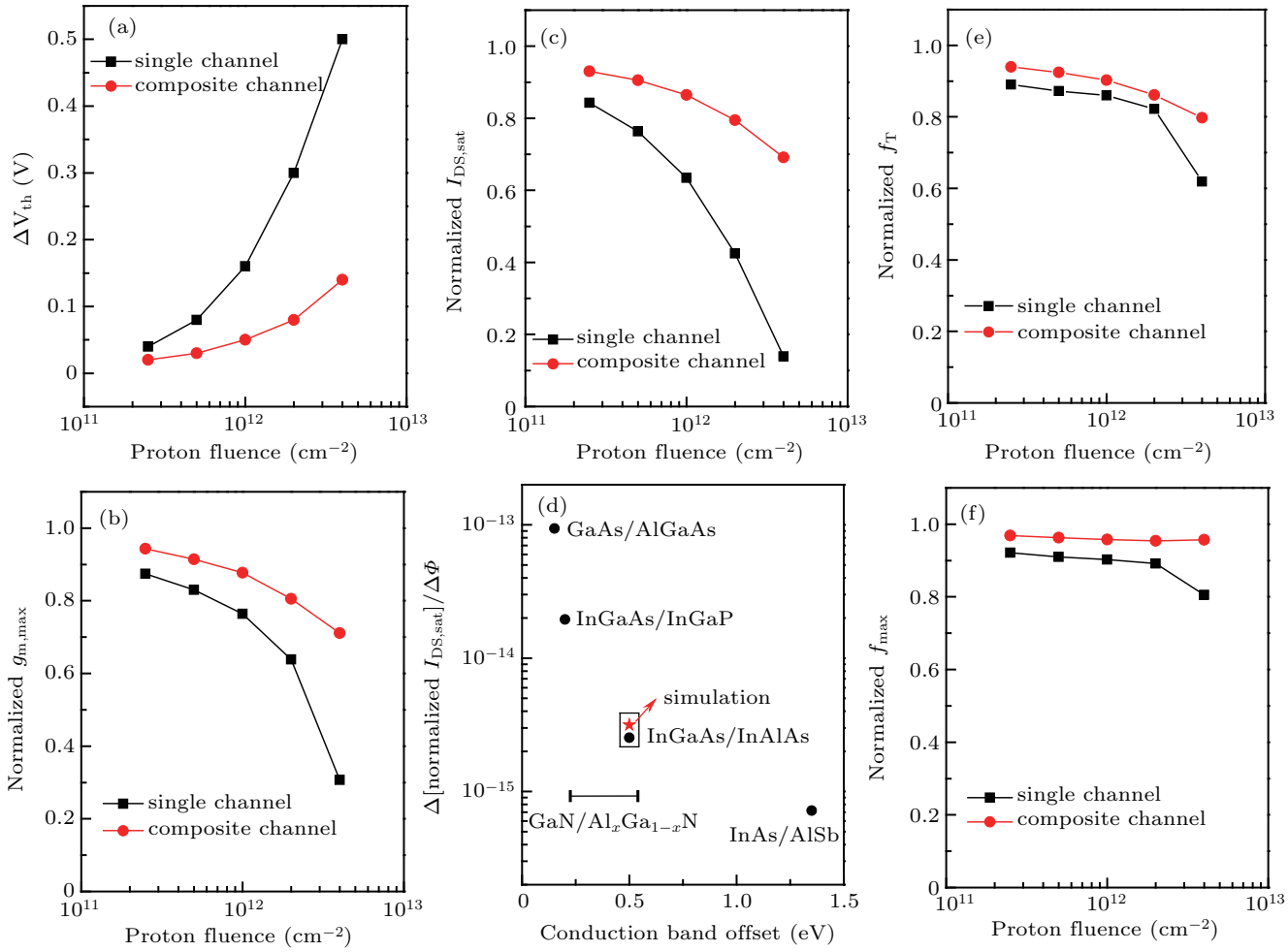


Fig. 6. Relationship between the normalized critical parameters and proton fluence: (a) $\Delta V_{\rm th}$, (b) normalized $g_{\rm m,max}$, (c) normalized $I_{\rm DS,sat}$, (e) normalized $f_{\rm T}$, (f) normalized $f_{\rm max}$, and (d) degradation rate of normalized $I_{\rm DS,sat}$ with equivalent fluence of 2-MeV proton *versus* conduction band offset for this simulation and various III–V HEMTs.[19]

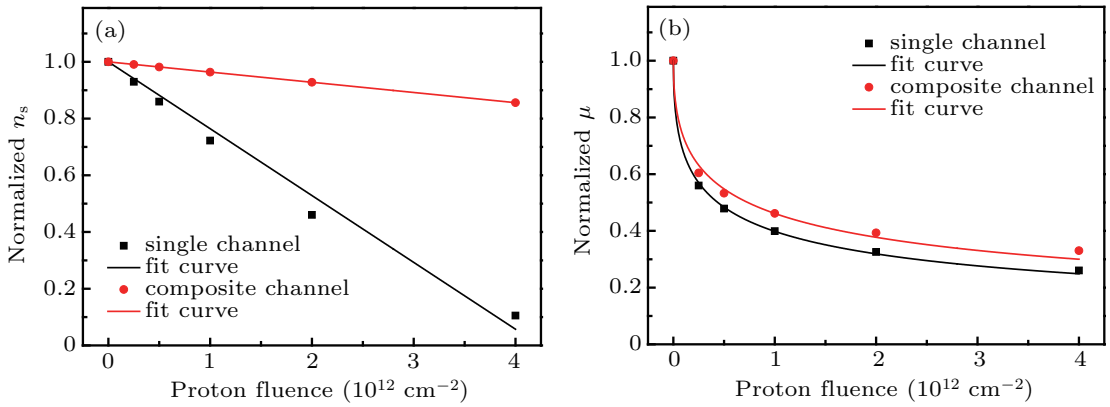


Fig. 7. (a) Normalized $n_{\rm s}$ and (b) normalized μ varying with proton fluence for single channel and composite channel.

The carrier removal effect of defects introduced by irradiation can be illustrated by extracting the capture rate of defects. Figure 8 shows the capture rates of different defect levels with respect to conduction band near the heterojunction region. Although the capture rates of the barrier layers are almost the same in both structures, there is a significant difference in channel layer because of the wide band-gap InAlGaAs subchannel. For a non-degenerate system, the probability of the defect levels occupied should follow the Boltzmann distribution function:

$$f(E_{\rm T}) = \exp\left(-\frac{E_{\rm T}-E_{\rm F}}{kT}\right). \tag{6}$$

Comparing with the band diagram of Fig. 4, the offset between the conduction band of the InAlGaAs subchannel and the Fermi level is about 0.3 eV. For the As vacancy defect energy level 0.15 eV adopted in this simulation,[32] the defects in the InAlGaAs subchannel are partially ionized. Comparing with the complete ionization of channel defects in the sin-

gle channel structure, the composite channel structure significantly reduces the carrier removal effect. This implies that through a reasonable composite channel structure, the device characteristics can be optimized while the radiation reliability can be improved.

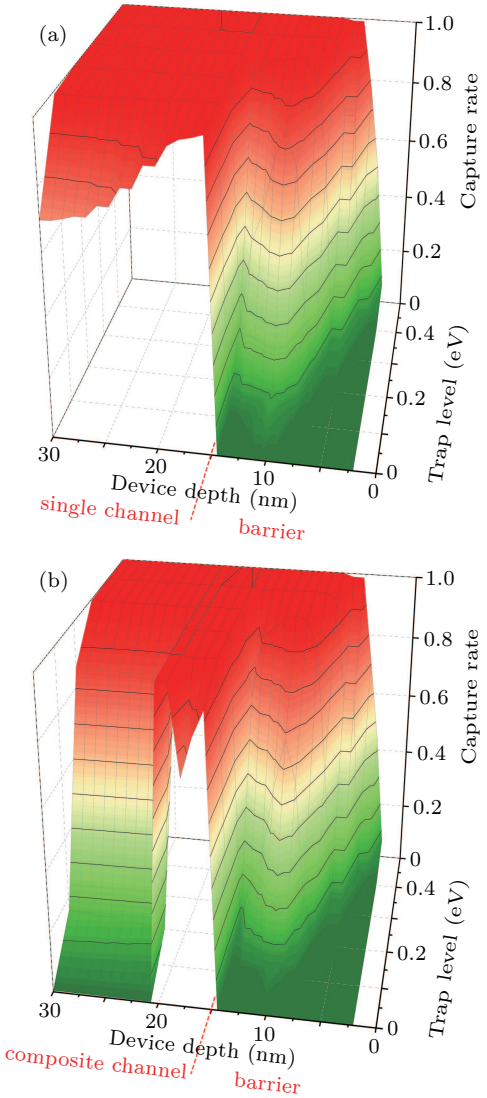


Fig. 8. Distribution of traps capture rate near heterojunction for (a) single channel structure and (b) composite channel structure.

3. Conclusions

In this work, a composite channel structure InP HEMT is proposed to improve the proton irradiation tolerance, and displays more excellent DC and RF characteristics than traditional single channel structure because of increased modulation doping efficiency and carrier confinement. Besides, the composite channel structure exhibits superior radiation reliability. By extracting the sheet density and mobility of two-dimensional electron gas, it is believed that the composite channel weakens the carrier removal effect. This can account for the increase of native carrier and the decrease of defect capture rate. Therefore, it is proved that a reasonable composite channel structure design can effectively improve the irradiation reliability of InP HEMT device.

References

[1] Sengupta K, Nagatsuma T and Mittleman D M 2018 *Nat. Electron.* **1** 622
[2] Chen Z, Ma X Y, Zhang B, Zhang Y X, Niu Z Q, Kuang N Y, Chen W J, Li L X and Li S Q 2019 *China Commun.* **16** 1
[3] Ma L H, Han W H and Yang F H 2020 *Chin. Phys. B* **29** 038104
[4] Ma L H, Han W H, Zhao X S, Guo Y Y, Dou Y M and Yang F H 2018 *Chin. Phys. B* **27** 088106
[5] Lei S G, Ma L L, Li M K, Peng W, Zhong Y H, Su Y F and Duan Z Y 2018 *J. Phys. D: Appl. Phys.* **51** 185603
[6] Mei X B, Yoshida W, Lange M, Lee J, Zhou J, Liu P H, Leong K, Zamora A, Padilla J, Sarkozy S, Lai R and Deal W R 2015 *IEEE Electron Dev. Lett.* **36** 327
[7] Cha E J, Wadefalk N, Moschetti G, Pourkabirian A, Stenarson J and Grahn J 2020 *IEEE Electron Dev. Lett.* **41** 1005
[8] Cha E J, Moschetti G, Wadefalk N, Nilsson P A, Bevilacqua S, Pourkabirian A, Starski P and Grahn J 2017 *IEEE T. Microw. Theory* **65** 5171
[9] Alt A R, Bolognesi C R, Gallego J D, Diez C, Lopez-Fernandez I and Barcia A 2011 *International Conference on Indium Phosphide and Related Materials,* May 22–26, 2011, Berlin, Germany, p. 1
[10] Ajayan J, Nirmal D, Ravichandran T, Mohankumar P, Prajoon P, Arivazhagan L and Sarkar C K 2018 *Int. J. Electron. Commun. (AE)* **94** 199
[11] Zhang Z, Cardwell D, Sasikumar A, Kyle E C H, Chen J, Zhang E X, Fleetwood D M, Schrimpf R D, Speck J S, Arehart A R and Ringel S A 2016 *J. Appl. Phys.* **119** 165704
[12] Lee I H, Polyakov A Y, Yakimov E B, Smirnov N B, Shchemerov I V, Tarelkin S A, Didenko S I, Tapero K I, Zinovyev R A and Pearton S J 2017 *Appl. Phys. Lett.* **110** 112102
[13] Chen J, Zhang E X, Zhang C X, McCurdy M W, Fleetwood D M, Schrimpf R D, Kaun S W, Kyle E C H and Speck J S 2014 *IEEE Trans. Nucl. Sci.* **61** 2959
[14] Petitdidier S, Guhel Y, Trolet J L, Mary P, Gaquiere C and Boudart B 2019 *IEEE Trans. Nucl. Sci.* **66** 810
[15] Meneghini M, Tajalli A, Moens P, Banerjee A, Stockman A, Tack M, Gerardin S, Bagatin M, Paccagnella A, Zanoni E and Meneghesso G 2017 *IEEE International Electron Devices Meeting*, December 2–6, 2017, San Francisco, USA, p. 753
[16] Sasaki H, Hisaka T, Kadoiwa K, Oku T, Onoda S, Ohshima T, Taguchi E and Yasuda H 2018 *Microelectron. Reliab.* **81** 312
[17] Zheng X F, Dong S S, Ji P, Wang C, He Y L, Lv L, Ma X H and Hao Y 2018 *Appl. Phys. Lett.* **112** 233504
[18] Zhang D L, Chen X H, Shen L Y, Zheng L, Gu Z Y, Liu X B and Yu Y H 2019 *IEEE Trans. Electron Dev.* **66** 2215
[19] Weaver B D, Martin P A, Boos J B and Cress C D 2012 *IEEE Trans. Nucl. Sci.* **59** 3077
[20] Weaver B D, Boos J B, Papanicolaou N A, Bennett B R, Park D and Bass R 2005 *Appl. Phys. Lett.* **87** 173501
[21] Jackson E M, Weaver B D, Shojah-Ardalan S, Wilkins R, Seabaugh A C and Brar B 2001 *Appl. Phys. Lett.* **79** 2279
[22] Sun S X, Liu H H, Yang B, Chang M M, Zhong Y H, Li Y X, Ding P, Jin Z and Wei Z C 2020 *Mater. Sci. Semicond. Proc.* **114** 105084
[23] Sun S X, Ji H F, Yao H J, Li S, Jin Z, Ding P and Zhong Y H 2016 *Chin. Phys. B* **25** 108501
[24] Sun S X, Ma L H, Cheng C, Zhang C, Zhong Y H, Li Y X, Ding P and Jin Z 2017 *Phys. Status Solidi A* **214** 1700322
[25] Zhong Y H, Yang B, Chang M M, Ding P, Ma L H, Li M K, Duan Z Y, Yang J, Jin Z and Wei Z C 2020 *Chin. Phys. B* **29** 38502
[26] Kalavagunta A, Touboul A, Shen L, Schrimpf R D, Reed R A, Fleetwood D M, Jain R K and Mishra U K 2008 *IEEE Trans. Nucl. Sci.* **66** 810
[27] Sun S X, Chang M M, Li M K, Ma L H, Zhong Y H, Li Y X, Ding P, Jin Z and Wei Z C 2019 *Chin. Phys. B* **28** 078501
[28] Ruiz D C, Saranovac T, Han D, Hambitzer A, Arabhavi A M, Ostinelli O and Bolognesi C R 2019 *IEEE Trans. Electron Dev.* **66** 4685
[29] Yamashita Y, Endoh A, Shinohara K, Hikosaka K, Matsui T, Hiyamizu S and Mimura T 2002 *IEEE Electron Dev. Lett.* **23** 573
[30] Jun B and Subramanian S 2002 *IEEE Trans. Nucl. Sci.* **49** 3222
[31] Gaudreau F, Fournier P, Carlone C, Khanna S M, Tang H P, Webb J and Houdayer A 2002 *IEEE Trans. Nucl. Sci.* **49** 2702
[32] Zhao J 1990 *IEEE Trans. Electron Dev.* **37** 2158